A preliminary numerical study on the existence of stable motions near the triangular points of the real Earth–Moon system

Àngel Jorba
Departament de Matemàtica Aplicada i Anàlisi
Universitat de Barcelona
Gran Via 585, 08007 Barcelona (Spain)
E-mail: `angel@maia.ub.es`

31st January 2000

Abstract

Let us focus on the motion of an infinitesimal particle moving near the triangular points of the real Earth–Moon system. Here, by real Solar system we refer to the model defined by the well-known JPL ephemeris. It is known that, from a practical point of view, the neighbourhood of the triangular points is unstable, in the sense that nearby particles escape after a short period of time.

In this paper we consider the existence of sets of solutions that remain near these points for a long time. To this end, we first use a simplified model (the so-called Bicircular Problem, BCP) that includes the main effects coming from Earth, Moon and Sun. The neighbourhood of the triangular points in the BCP model is unstable, as it happens in the real system. However, here we show that, in the BCP, there exist sets of initial conditions giving rise to solutions that remain close to the Lagrangian points for a very long time spans. These solutions are found at some distance of the triangular points.

Finally, we numerically show that some of these solutions seem to subsist in the real system, in the sense that the corresponding trajectories remain close to the equilateral points for at least 1000 years. These orbits move up and down with respect to the Earth–Moon plane, crossing this plane near the triangular points. Hence, as it is discussed in the paper, the search for Trojan asteroids in the Earth–Moon system should be focused on these regions and, more concretely, in the zone where the trajectories reach their maximum elongation with respect to the Earth–Moon plane.

Keywords: Lagrangian points, Trojan motion, effective stability, lower dimensional tori, quasi-periodic orbits.

Contents

1 Introduction

To introduce the problem considered in this paper, let us start by recalling the definition of the Restricted Three Body Problem (from now on, RTBP). Let us start by assuming that Earth and Moon are point masses that revolve in circular orbits around their common centre of masses. Let us consider a particle with infinitesimal mass under the gravitational attraction of Earth and Moon (in this context, Earth and Moon are sometimes called "primaries"). With infinitesimal mass we mean that we are neglecting the gravitational attraction of this third particle on the primaries, so they keep describing a circular orbit. The study of the dynamics of this third particle is the so-called RTBP.

It is usual to take a system of reference with the origin at the centre of masses, and with rotating axes such that the primaries are fixed on the x axis, the y axis is contained in the plane of motion of the primaries and orthogonal to the x axis, and the z axis is orthogonal to the (x, y) plane. The x axis is oriented from the smallest to the biggest primary, the z axis is oriented as the angular momentum of the circular motion of the primaries, and the y axis is oriented to obtain a positive-oriented frame. The unit of distance is defined as the distance between primaries, the unit of mass is defined as the total mass of the primaries, and the unit of time is such that the gravitational constant is one. In these units, the period of the primaries around their common centre of mass is equal to 2π. This system of reference is usually called synodical. In this system of reference, Earth and Moon have coordinates $(\mu, 0, 0)$ and $(\mu - 1, 0, 0)$, respectively. It turns out that the equations of motion of the infinitesimal particle can be written in Hamiltonian form, with Hamiltonian function given by

$$H_{RTBP} = \frac{1}{2}(p_x^2 + p_y^2 + p_z^2) + yp_x - xp_y - \frac{1-\mu}{r_{PE}} - \frac{\mu}{r_{PM}}, \tag{1}$$

being $r_{PE}^2 = (x-\mu)^2 + y^2 + z^2$ the distance of the particle to the Earth, and $r_{PM}^2 = (x - \mu + 1)^2 + y^2 + z^2$ the distance of the particle to the Moon.

It is well known that, in synodical coordinates, the RTBP has five equilibrium points, three of them lay on the x axis (they are also called Euler points, collinear points or simply L_1, L_2 and L_3) and two of them are the third vertex of an equilateral triangle that has the primaries as the other vertices (they are also called Lagrangian points, triangular points or L_4 and L_5). The position of these points has been marked in Figure 1. For more details see, for instance, [21] or [26].

Let us start by focusing on the dynamics around the equilateral points $L_{4,5}$ of the RTBP. To simplify the discussion, we will start discussing the L_5 point (for the RTBP, the same results will hold for L_4 due to the symmetries of this model). For the value of the masses corresponding to the Earth–Moon case, L_5 is an elliptic equilibrium point. Under very general conditions, standard results from KAM theory (for a survey, see [2]) predict that, around an elliptic equilibrium point of a Hamiltonian system, there exist plenty of quasi-periodic solutions. In suitable coordinates (the so-called action-angle variables), these solutions correspond to linear motions taking place on invariant tori, whose dimension coincides with the number of basic frequencies of the quasi-periodic motion. For this reason, in this context it is usual to refer to quasi-periodic solutions as invariant

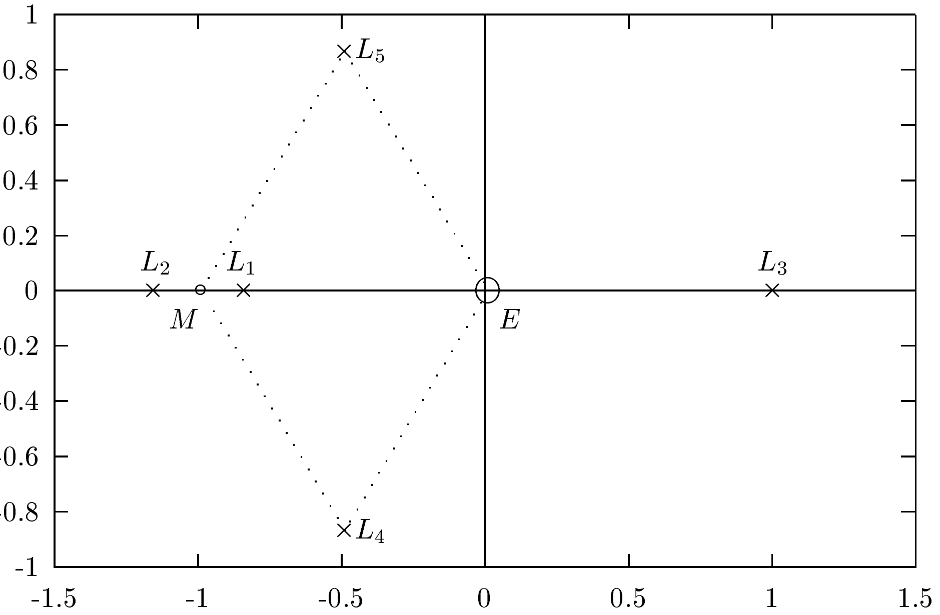

Figure 1: The five equilibrium points of the RTBP.

tori. Due to the constraints imposed by the Hamiltonian structure, the dimension of these tori (as well as the number of basic frequencies of the quasi-periodic motions) cannot be greater than half the dimension of phase space. In this sense, we will distinguish between maximal dimensional tori (tori whose dimension equals half the dimension of phase space) and lower dimensional tori. It is well known that the set filled by these tori has positive measure and empty interior. Obviously, initial conditions inside this set give rise to trajectories that are always close to the equilibrium point. Hence, to study the instability of an elliptic point we should look at the dynamics on the complementary of the tori set. The (possible) diffusion inside this set is usually called Arnol'd diffusion (it was first conjectured by Arnol'd in [1]), and it is actually one of the major open problems in the Hamiltonian dynamics field. The main results in this direction are only upper bounds on the diffusion speed (see [2]). For concrete estimates around elliptic equilibrium points of autonomous systems see, for instance, [9], [24], [5], [17], and [3]. One of the main conclusions of these works is that, under general conditions, the time needed to escape of a neighbourhood of the equilibrium point is (at least) exponentially big with respect to the distance of the initial condition to the equilibrium point. Hence, the application of these results to the RTBP corresponding to the Earth–Moon case results in very large stability times. This kind of stability is usually called effective stability.

On the other hand, let us consider the motion of a particle in the real Solar system, close to the triangular points of Earth and Moon. Before continuing, let us give a precise definition of what we understand by "real Solar system". Let us first assume that we know the position of Earth, Moon, Sun and planets. From this data, we can easily compute the gravitational attraction of these bodies on a particle sitting in any point of space. This is a numerically defined vector field, that we can integrate (numerically) for the time span for which the positions of the main bodies is known. In other words, we assume that the Solar system evolves in a given (and known) way, and we compute the motion of the particle under the attraction of these bodies. For the positions of the main bodies of the Solar system we use one of the most accurate sets of data available: the JPL ephemeris [27]. More concretely, we have used the file DE406, that is defined from the Julian day 625360 (February 23rd, 3000 BC) to the Julian day 2816848.5 (March 3rd, 3000 AD). Note that, for the real system, the triangular points are not longer equilibrium points since the hypotheses used to derive the RTBP are not exactly satisfied. It is known that arbitrary trajectories starting near the (geometrically defined) triangular points go away after a short time (see [7] and references therein) and hence, the RTBP is not a good model to study this problem because it displays a quite different qualitative behavior.

For this reason, we will start using the so called Bicircular Problem (from now on, BCP). This model can be seen as a time dependent periodic perturbation of the RTBP, that includes the main effect coming from the Sun. As far as we know, this model was first introduced in [26]. As we will see, the BCP has some of the main features of the real model (for instance, the neighbourhood of the equilateral points is unstable). Our purpose is to use the BCP as a first model to describe some properties of the real system. In particular it is known that the BCP has families of 2-D invariant tori near the equilateral points (see [4]). It turns out that some of these tori are hyperbolic, while some others are elliptic ([15]), and that those elliptic tori are found at some distance from the equilateral points. It is known that lower-dimensional normally elliptic tori give rise, under general conditions, to regions of effective stability around them (see [18], [17]). Here, we will estimate the size and shape of these regions by means of numerical simulations, to show that they are relevant for this problem.

The last step will be to show, by means of numerical simulations, that some of the stability regions found in the BCP model subsist in the real system, at least for time spans of 1000 years. As it will be discussed later (in Section 5), these regions are a suitable place to look for Trojan asteroids in the Earth–Moon system.

Finally, let us mention that this kind of stability was already observed in [11] (see also [25]), but with smaller regions and much shorter time intervals (around 60 years). The main improvements in this work come from the computation of the vertical families of 2-D tori for the BCP and to use initial conditions around them. It seems that these families of tori are the skeleton that supports these stability regions.

A preliminary version of the results in this paper was presented in [14].

2 The Bicircular model

The bicircular model is a modification of the RTBP, in order to take into account (in an approximate way) the effect of the Sun. In this model, Earth and Moon move in circular orbits around their centre of masses (as in the RTBP), and this centre of masses is moving around the Sun, that is fixed at the origin. Then, it is not difficult to derive the equations of motion of an infinitesimal particle moving under the attraction of these three bodies. The study of the motion of this particle is the so-called Bicircular Problem (from now on, BCP). It is usual to take the same reference frame (and normalized units) as in the

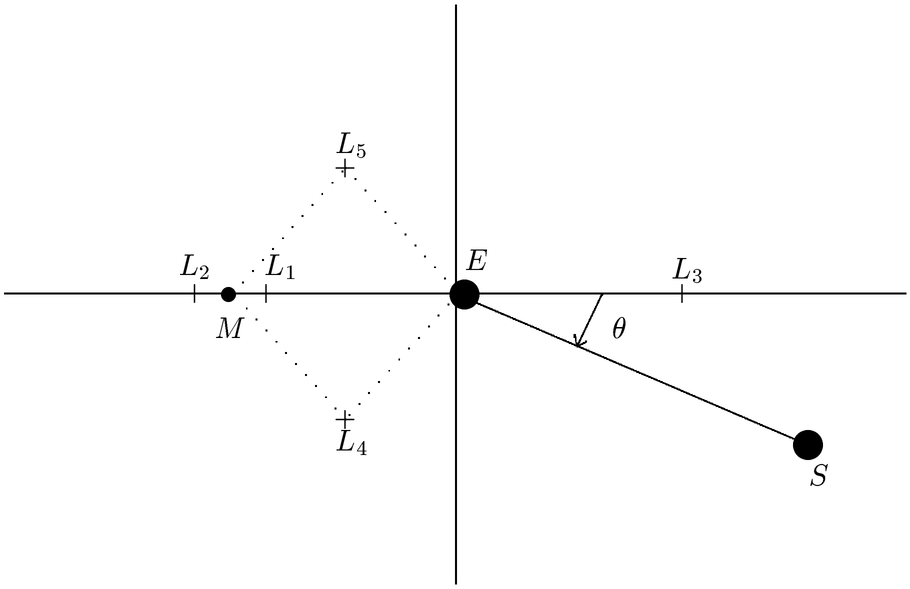

Figure 2: The Bicircular Problem.

μ	$=$	0.012150581623433623	m_S	$=$	328900.54999999906
ω_S	$=$	0.925195985518289646	a_S	$=$	388.81114302335106

Table 1: Floating point values used for the different constants of the BCP. Not all the digits are significative (they appear because the definition of these quantities involves quotients).

RTBP, that is, the origin is at the centre of masses of the Earth-Moon system, the x axis is on the Earth-Moon line, and so on. Hence, in this system of reference, the Sun is turning around the origin in a periodic way (see Figure 2).

Defining momenta as $p_x = \dot{x} - y$, $p_y = \dot{y} + x$ and $p_z = \dot{z}$, then the motion of the infinitesimal particle can be described by a Hamiltonian system that depends on time in a periodic way:

$$\begin{aligned} H_{BCP} &= \frac{1}{2}\left(p_x^2 + p_y^2 + p_z^2\right) + yp_x - xp_y - \\ &\quad -\frac{1-\mu}{r_{PE}} - \frac{\mu}{r_{PM}} - \frac{m_S}{r_{PS}} - \frac{m_S}{a_S^2}\left(y\sin\theta - x\cos\theta\right), \end{aligned} \tag{2}$$

where $r_{PE}^2 = (x-\mu)^2+y^2+z^2$, $r_{PM}^2 = (x-\mu+1)^2+y^2+z^2$, $r_{PS}^2 = (x-x_S)^2+(y-y_S)^2+z^2$, $x_S = a_S\cos\theta$, $y_S = -a_S\sin\theta$, and $\theta = \omega_S t$. The values used for these constants are listed in Table 1. We stress that the BCP can be written as a periodic time dependent perturbation of the RTBP:

$$H_{BCP}^{\varepsilon} = H_{RTBP} + \varepsilon\widehat{H}_{BCP}, \quad \widehat{H}_{BCP} = -m_S\left(\frac{1}{r_{PS}} + \frac{y\sin\theta - x\cos\theta}{a_S^2}\right), \tag{3}$$

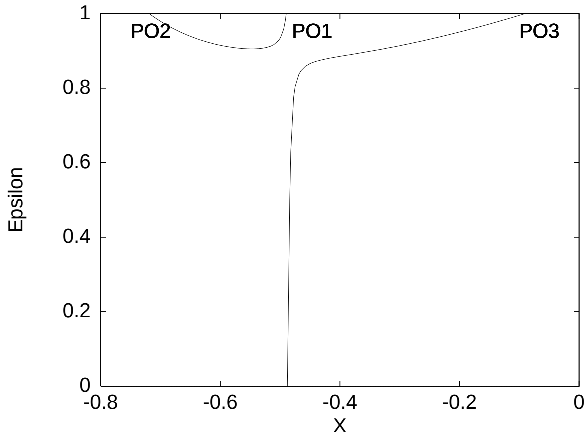

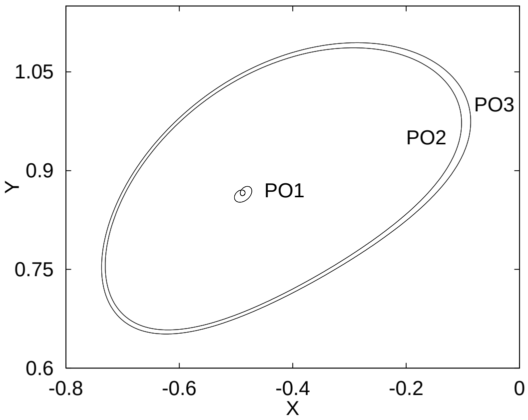

Figure 3: Left: Continuation of the periodic orbit that replaces L_5 in the BCP. Right: The three periodic orbits that appear in the left plot for $\varepsilon = 1$.

and it is clear that $H_{BCP}^{\varepsilon=0} = H_{RTBP}$, and that $H_{BCP}^{\varepsilon=1} = H_{BCP}$.

Now, let us focus on the L_5 point (due to the symmetries of the RTBP and the BCP, the same results will be valid for L_4; of course, this is not true for the real system). As the vector field of the perturbation $\varepsilon \widehat{H}_{BCP}$ does not vanish on L_5, this point is not longer an equilibrium solution. An straightforward application of the Implicit Function Theorem shows that, under a generic non-resonance condition (satisfied in this case) and assuming ε small enough, L_5 is replaced by a periodic orbit with the same period as the perturbation. This orbit tends to L_5 when ε tends to zero.

Let us consider now the Poincaré section defined by $t = 0 \mod T_S$, where $T_S = 2\pi/\omega_S$ is the period of the perturbation. Let us call P_ε the corresponding Poincaré map. Note that the fixed points of this map correspond to periodic orbits (of period T_S) for the flow, and vice versa.

Now, by means of a continuation process, let us compute the fixed points of P_ε (for ε ranging between 0 and 1) that correspond to the periodic orbit that replaces L_5. The results are displayed in Figure 3 (left), where the horizontal axis shows the x coordinate of the fixed point and the y coordinate refers to the value of ε. Note that, for $\varepsilon = 1$, there are three fixed points of P_ε that are close to L_5. The (x, y) projection of the corresponding periodic orbits for the flow are displayed in Figure 3 (right).

By computing the eigenvalues of the differential of P_ε at the fixed points, one can see that orbit PO1 is unstable, and that orbits PO2 and PO3 are linearly stable (see Figure 3). Moreover, the three periodic orbits have an elliptical mode contained in the (z, p_z) plane. In what follows, we will refer to this mode as the vertical mode of the corresponding periodic orbit. For more details about the BCP, see, for instance, [11] or [25].

2.1 The vertical families of 2-D tori of the BCP

Let us now consider the vertical mode of one of the periodic orbits. It is known that, under generic conditions (see [18], [17]), there exists a Cantor family of 2-D invariant tori that extend this linear mode into the complete (i.e., nonlinear) system. This is very similar

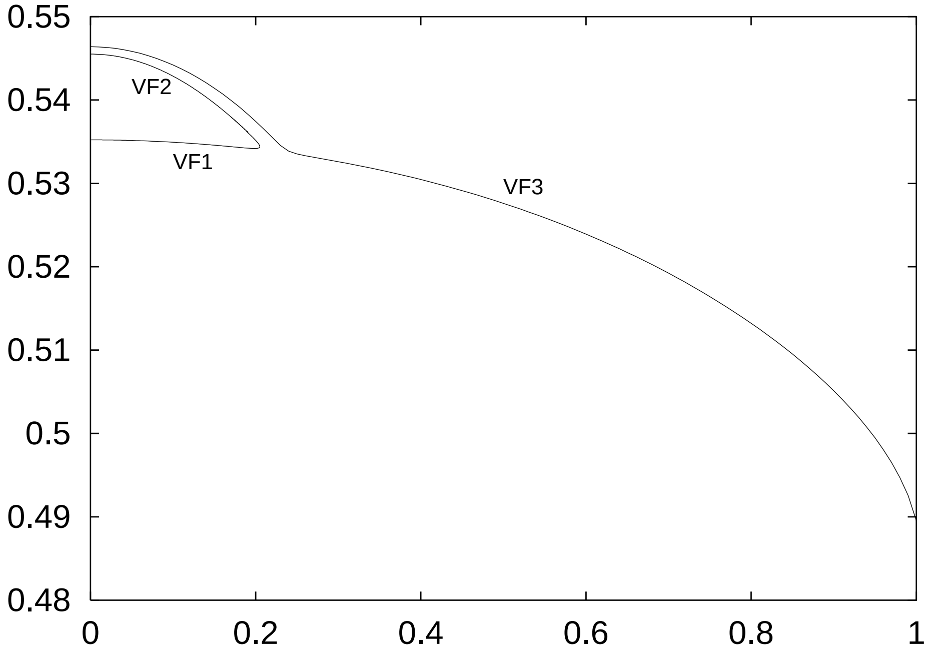

Figure 4: The vertical families of 2-D tori. The graphic corresponds to the map P_ε. The horizontal axis contains the $\dot{z}$ coordinate, and the vertical axis displays the rotation number. See the text for more details.

to the well-known Lyapunov centre theorem: instead of obtaining a (smooth) family of periodic orbits, one obtains a (Cantor) family of 2-D tori. Hence, for each periodic orbit PO1, PO2 and PO3, there is a Cantor family of tori (let us call them VF1, VF2 and VF3, respectively) that "grows up" in the vertical direction.

In order to display these families, we use again the map P_ε defined before. In this way the 2-D tori become invariant curves of a 6-D symplectic map. As all these curves cross the hyperplane $z = 0$ we select, for each curve, the only point on the invariant curve that has $z = 0$ and $\dot{z} > 0$. In this way, every curve is represented by a single point. We have used this representation in Figure 4. The horizontal axis displays the $\dot{z}$ coordinate while the vertical axis contains the rotation number of the invariant curve. Note that families VF1 and VF2 are connected (as suggested by the connection of the periodic orbits PO1 and PO2 in Figure 3), while F3 reaches high amplitudes in the $(z, \dot{z})$ direction. More details about these computations can be found in [4].

It is also known that, under generic hypotheses of non-resonance, the tori on these families that are close to the basic periodic orbits have the same stability as them. So, for moderate vertical amplitudes, we expect the tori on VF1 to be hyperbolic, and most of the tori on VF2 and VF3 to be elliptic. Families VF1 and VF2 are connected through a turning point, and this is where the change of stability takes place. Family VF3 can be continued up to very high values of the vertical amplitude and, except for small intervals of instability (produced by some resonances), the tori in this family are normally elliptic.

For more details on the normal stability of these families see [14] and [15].

It is known that normally elliptic lower dimensional tori are surrounded by a region of effective stability ([17]). This means that the time needed to escape from a neighbourhood of one of those tori increases exponentially with the initial distance to the torus. A possibility to estimate the size of this region and the speed of diffusion is to compute a normal form around the torus and to derive estimates on the remainder (for examples of this technique around periodic orbits, see [16] and [19]). Of course, the obtention of "analytical" bounds usually requires the use of rather pessimistic inequalities that lead us to underestimate the region where the diffusion is small enough. Here, to have a realistic estimate of the size and shape of this region, we will simply use a numerical simulation to detect initial conditions for which the corresponding trajectory remains there for a sufficiently large time interval. In what follows, we will use the words "quasi-stable region" to refer to a region such that the time taken to escape from it is bigger than a large prescribed value (this value will be specified later).

2.2 Numerical simulations

Let us fix our attention on a given 2-D torus on one of these families. To reduce the number of degrees of freedom of the problem, we will use the Poincaré section $t = 0$ and the map P_ε defined before. In this section, the tori in the families VF1, VF2 or VF3 become invariant curves. Let us select the (unique) point a_0 on the curve such that $z = 0$ and $\dot{z} = \dot{z}_0 > 0$ (the value $\dot{z}_0$ will be used as a parameter). The next step is to select a mesh of initial conditions around the point a_0. To reduce the computations, we will use a two dimensional mesh as follows: we fix the coordinates z, p_x, p_y and p_z to the corresponding values of a_0, and the values of x and y are used as parameters. Due to the shape of this regions (this will be clear later on), we will use the following grid:

$$\left\{ \begin{array}{rcl} x_{ij} & = & r_i \cos\alpha_j + \mu, \\ y_{ij} & = & r_i \sin\alpha_j, \end{array} \right. \qquad \begin{array}{rcl} r_i & = & 1 + ih_r, \\ \alpha_j & = & 2\pi j h_\alpha, \end{array} \tag{4}$$

where h_r and h_α are used to select the density of the mesh and the (integer) indices i and j move on suitable ranges. Then, we will use each point on the grid as initial condition for a numerical integration of the vector field of the BCP. To decide if the trajectory escapes, after each time step of the numerical integrator (see Section 4), the program uses a couple of tests. First, it checks the actual distance to Earth and Moon. If the distance to the primaries is lower than their respective radius, then the initial condition is not considered as belonging to the quasi-stable region. The second test is to check whether the actual point has crossed the $y = -0.5$ plane (we recall that we are working around the L_5 point). Numerical experiments show that this last condition is equivalent to escape. This has already been used before (sometimes with different values for the y section) in several works, see [11], [25].

In this paper, we have used the values $h_r = 0.001$ and $h_\alpha = 0.0002$. The different sizes between these two values is to produce a nearly squared grid. For the numerical integrations we have used a time interval of 15000 Moon revolutions (we recall that, in the BCP model, this is equivalent to $15000 \times 2\pi$ units of time).

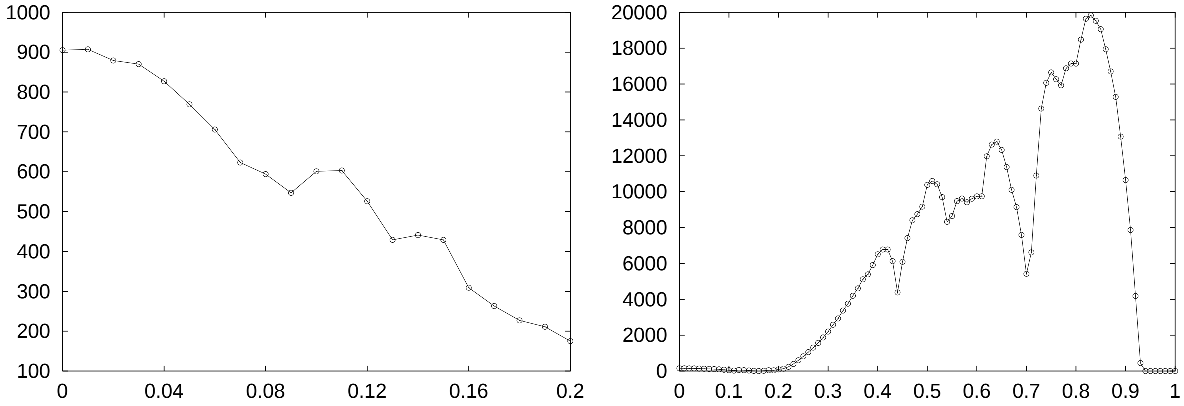

Figure 5: Estimation of the size of the quasi-stable region for the BCP model. The horizontal axis shows the value of $\dot{z}$ (see the text), and the vertical axis contains the number of points inside the quasi-stable region. Left: Family VF2. Right: Family VF3.

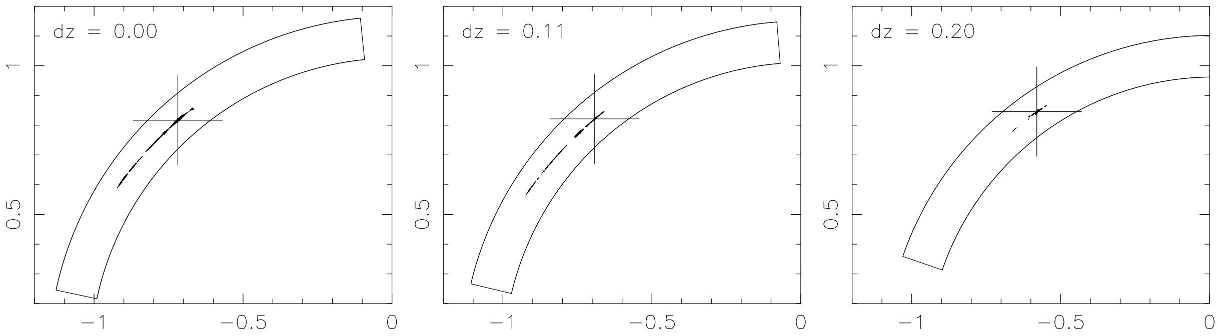

Figure 6: Slices of the quasi-stability regions around the Family VF2 in the BCP. The horizontal and vertical axis are the x and y coordinates, respectively. The central quasi-periodic trajectory has been marked with a big "+" sign.

The results are summarized in Figure 5 for the VF2 and VF3 families. The horizontal axis displays the same value of $\dot{z}$ used in the previous section (see also the horizontal axis of Figure 4). The vertical axis displays the number of non escaping points after 15000 Moon revolutions. As we have always used the same mesh, the number of non escaping points is a good estimate of the size of the stable region. For the Family VF2 the region is not very big, and its size decreases when the value of $\dot{z}$ increases; this is very natural since Family VF2 becomes hyperbolic when it meets VF1 (more details in [14] and [15]). Family VF3 has a bigger stability when $\dot{z}$ ranges from 0.26 and 0.92 (when $\dot{z}$ is below 0.20, the size of the region associated to VF3 is in fact smaller than the VF2 one).

Figure 6 contains a few slices of the stability region around VF2. The big cross in the graphic denotes the intersection of the invariant curve with this slice. The region explored has been drawn with a semi-circular box.

Several slices for Family VF3 are displayed in Figure 7. These slices correspond to the biggest parts of the region (see Figure 5). We recall that that the unit of distance in these plots is the Earth–Moon distance, so the size of the displayed regions is quite big in

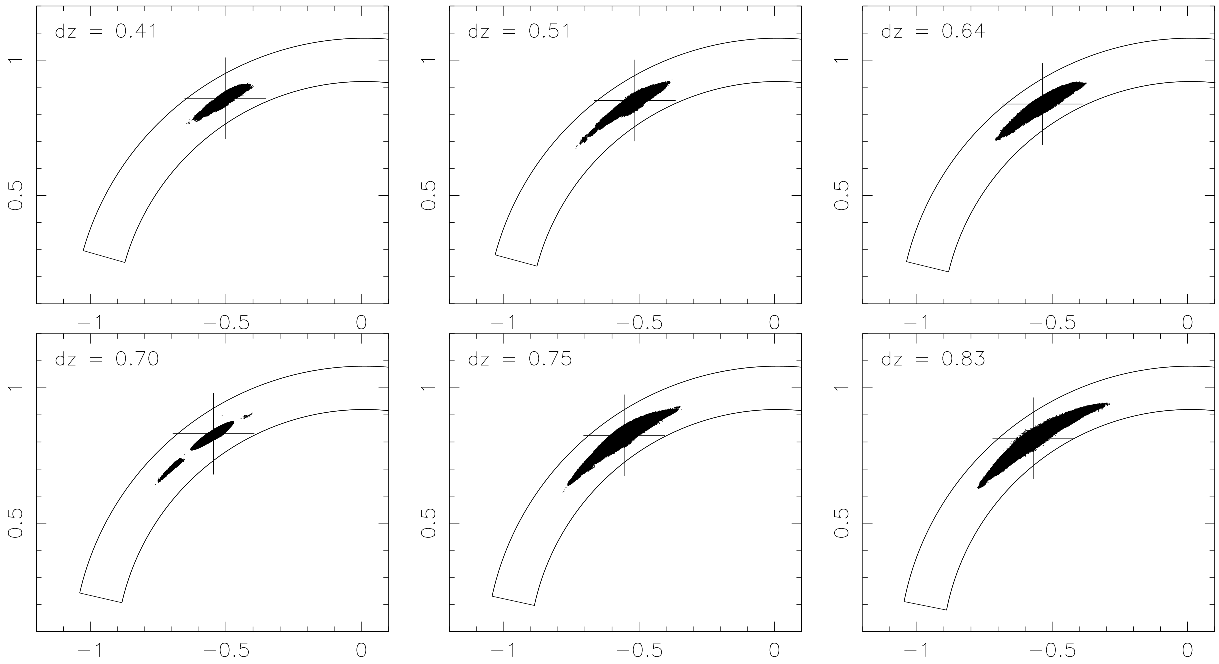

Figure 7: Slices of the quasi-stability regions around the Family VF3 in the BCP. The horizontal and vertical axis are the x and y coordinates, respectively. The central quasi-periodic trajectory has been marked with a big "+" sign.

the physical system. As it has been mentioned before, it is worth noting that the biggest part of the region correspond to high values of the $\dot{z}$ coordinate.

2.3 Remarks

As it has been explained before, the computation of the vertical families of quasi-periodic solutions has been done on the map P_ε. In this way, what we have obtained is an invariant curve, that can be seen as the intersection of the corresponding 2-D torus with the plane $t = 0 \bmod 2\pi$.

In order to reduce the number of numerical simulations, we have restricted the search of the stable region by selecting a single point on the invariant curve (the one having $z = 0$ and $\dot{z} > 0$), and taking a 2-D mesh around this point. This mesh is obtained by moving the (x, y) values of this point and keeping the remaining coordinates constant. Note that this process produces a very concrete slice of the stable region. The computation of the full region would require a 5-D mesh, obtained by moving 5 coordinates around the initial point ($\dot{z}$ should be kept fixed to avoid changing the base invariant curve). Of course, we can apply this process to every curve on the family (i.e., moving $\dot{z}$), and this will produce an estimate of the full (6-D) region for the map P_ε. The total region for the BCP still requires to take all the points of the stable region for P_ε as initial conditions, and to integrate them for a period of the time variable t. This would produce a 7-D region inside the 7-D phase space. In other words, the 2-D slice that we have computed in the previous section is the result of taking the full 7-D region for the BCP when $t = 0$ (a

6-D section), fix $z = 0$ (5-D section), and fix $\dot{z}$ and the momenta p_x and p_y to suitable values to define the final 2-D slice. The computation of the 7-D quasi-stable region would require a prohibitive amount of computer time. This is the main reason to restrict the simulations to the 2-D slice defined above.

3 The JPL model

In this section we will check the quasi-stability results for a very realistic model of Solar system. The model used here is defined by the Jet Propulsion Laboratory (JPL) ephemeris ([27]), file DE406. The JPL ephemeris are files containing interpolatory polynomials for the orbital data of each planet, including Sun, Earth and Moon. This data can be easily used to derive the vector field acting on an infinitesimal particle under the attraction of the main bodies of the Solar system. Of course, this numerically obtained vector field is only valid for the time interval for which the ephemeris are provided.

3.1 Numerical simulations

The initial time for the numerical integration is the modified Julian day 20.1978749133 (day 0.0 corresponds to year 2000.0), that coincides with the first full Moon of year 2000.[1] This is to have an initial relative position of Earth, Moon and Sun similar to the one of the BCP for $t = 0$. The simulation stops at year 3000.0. We have also used the same mesh as in the BCP model (see Section 2.2). Due to the lack of symmetry between L_4 and L_5 in the real system, we have done simulations for both cases. The obtained results are very similar, and are discussed in the following sections.

3.1.1 Stability around the family VF2

In order to compare this results with the ones of the BCP, we have used the same mesh as in Section 2.2. Figure 8 shows the number of initial conditions corresponding to trajectories that do not escape (in the same sense as in Section 2.2) for time spans of 10 years (upper curve) and 100 years (lower curve).

We do not include the results for 1000 years because only a few trajectories subsist. In the L_4 case, the number of these points is never greater than 8, while for the L_5 case this number is slightly bigger: the more stable section corresponds to the case $\dot{z} = 0.13$, that contains 85 surviving points. From these results, and concerning the behaviour around the family VF2, L_5 it seems that is slightly more stable than L_4. Moreover, if the integration time is long enough, we believe that all these trajectories will finally escape.

Note the size of the quasi-stable region for a time interval of 10 years (see Figures 9 and 10). Although a stability time of 10 years is totally irrelevant for astronomical purposes, it could be interesting for astronautical applications, since there is no need of any kind of control to keep an spacecraft there. The strategy to transfer a spacecraft from a parking

[1] In fact, this is the date of the first lunar eclipse of year 2000.

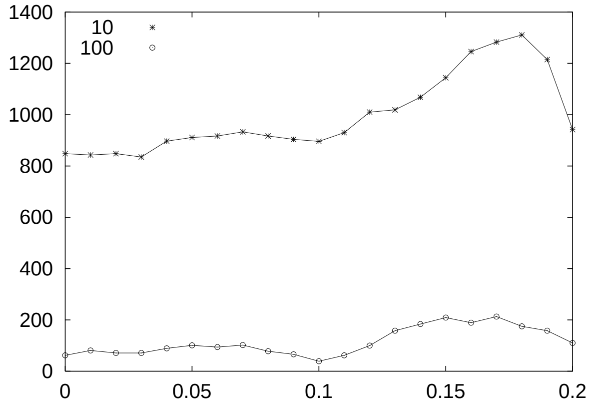

Figure 8: Estimation of the size of the quasi-stable region corresponding to the family VF2 for the JPL model. The upper curve (marked with $*$) is for an integration time of 10 years. The lower curve (marked with $\circ$) corresponds to an integration time of 100 years. Left: L_4 case. Right: L_5 case. See the text for more details.

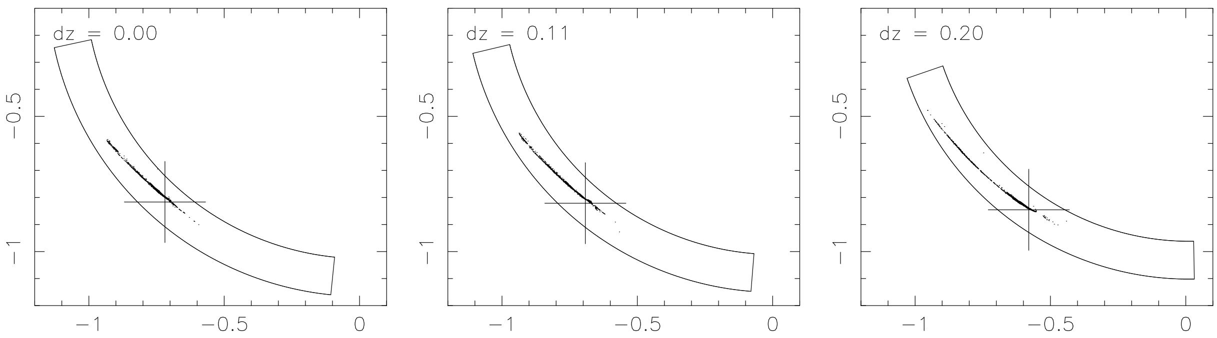

Figure 9: Quasi-stability regions (for a time interval of 10 years) near L_4 around the Family VF2 in the JPL model.

orbit to these regions is not considered here.[2] For a dynamical systems approach to similar transfers, see [11], [6].

3.1.2 Stability around the family VF3

This family seems to be responsible for the biggest quasi-stability regions we have found near the Lagrangian points. Figure 11 shows the number of initial condition corresponding to non escaping trajectories (this is the same plot as in Figure 5 but for the JPL model). As we have used the same parameters to define the mesh of initial conditions, the "units" in those plots –the vertical axis– are also the same. So, although the stability region is smaller in the JPL model compared with the BCP model, it is remarkable that there exists a quite large stability region for a time span of 1000 years. In order to compare with

[2]Roughly speaking, a transfer by means of a double lunar swing-by from the standard Arianne Geostationary Transfer Orbit to the vicinity of the triangular points can be completed in about 2 months using a little bit less than 900 m/s of Δv; see [6] for more details.

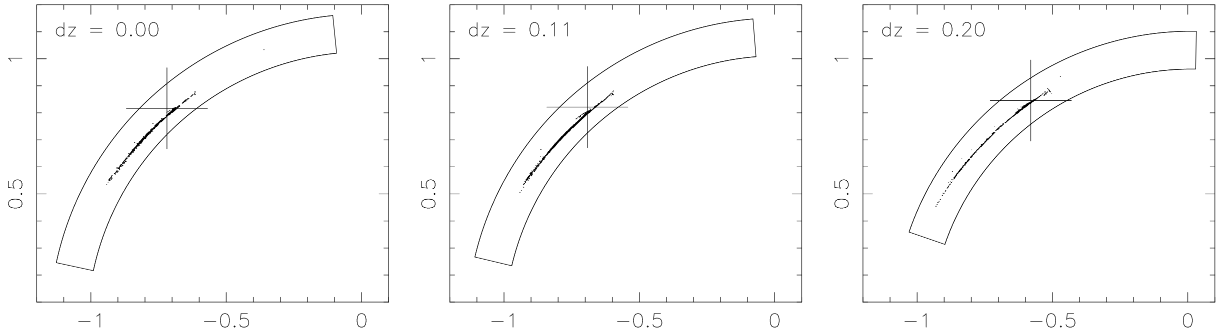

Figure 10: Quasi-stability regions (for a time interval of 10 years) near L_5 around the Family VF2 in the JPL model.

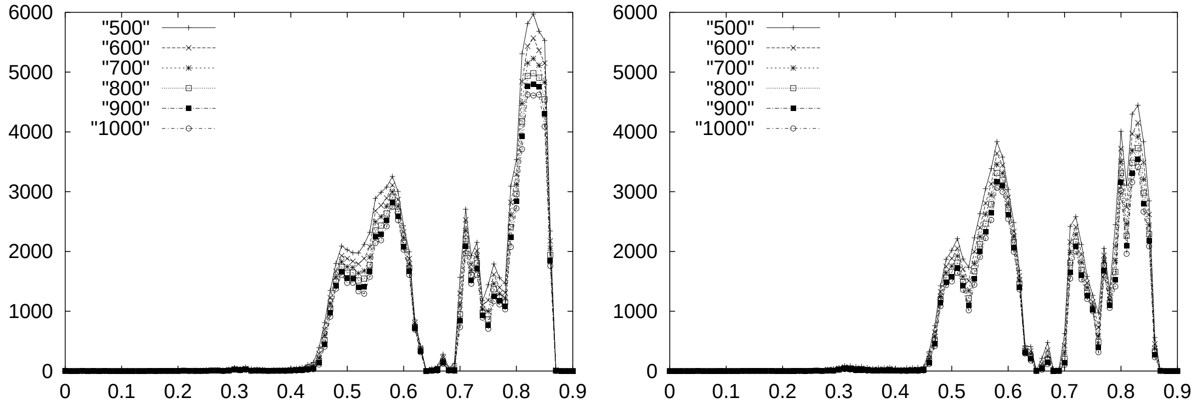

Figure 11: Estimation of the size of the quasi-stable region corresponding to the family VF3 for the JPL model. The plot contains different curves corresponding to several quasi-stability times, ranging from 500 (upper curve) to 1000 years (lower curve). Left: L_4 case. Right: L_5 case. See the text for more details.

the simulations for the BCP model, note that 1000 years is more than 13000 revolutions of the Moon around the Earth.

Figures 12 and 13 show the (x, y) coordinates of a few slices of the quasi-stability region for a time interval of 1000 years, near the triangular points L_4 and L_5 respectively. The selected slices correspond to places in which the region is quite big, according to Figure 11. We recall that the unit of distance is the Earth-Moon distance for the MJD 20.1978749133, that is, about 384467 Km.

From these plots, it seems clear that the BCP model contains several features of the JPL system. This is specially true concerning to the location of quasi-stability regions, as it has been shown by these calculations. However, comparing Figures 5 (right) and 11 it is also clear that not all the features of JPL are present in BCP. We believe that these differences are mainly due to resonances in JPL that are not present in BCP, due to the simplicity of the latter. The development and study of better models is actually work in progress.

It is clear that the size of these regions could depend on the length of the integration

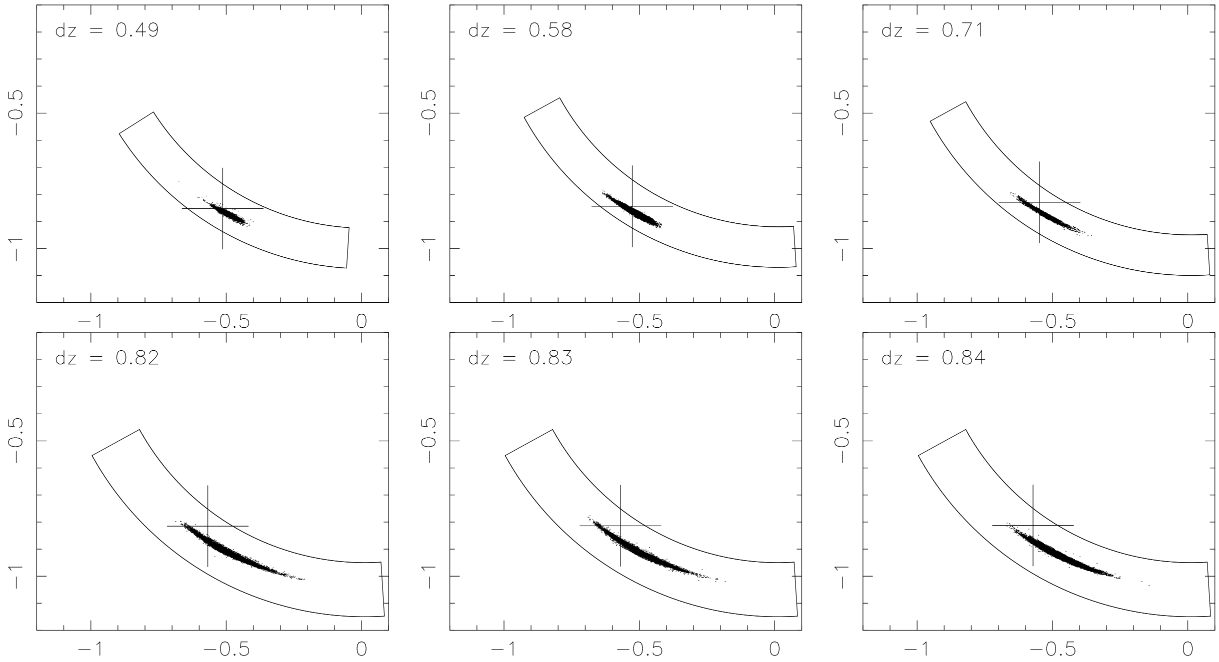

Figure 12: Quasi-stability regions (for a time interval of 1000 years) near L_4 around the Family VF3 in the JPL model.

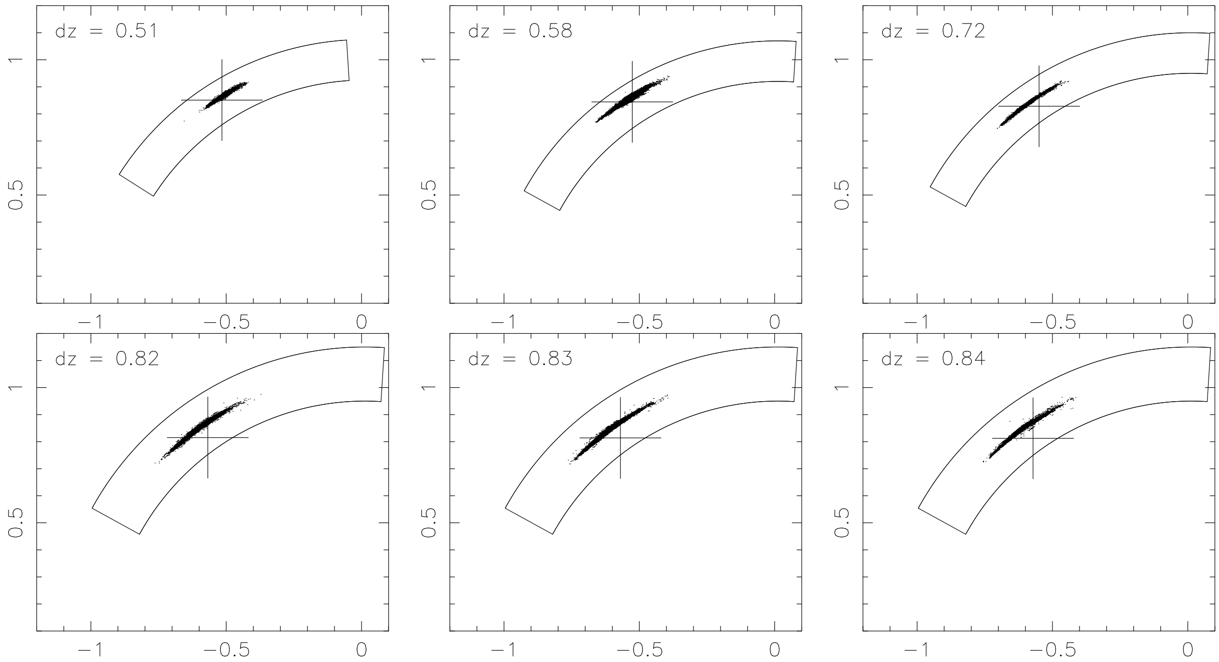

Figure 13: Quasi-stability regions (for a time interval of 1000 years) near L_5 around the Family VF3 in the JPL model.

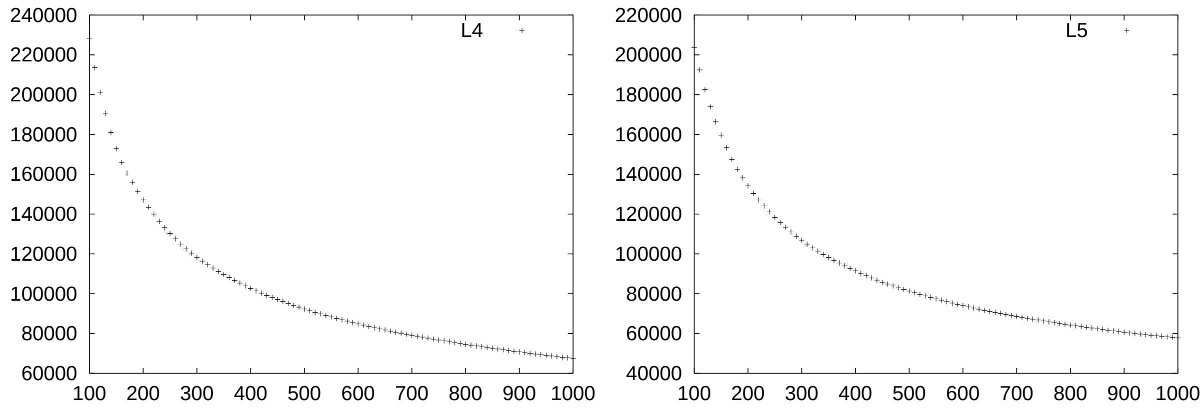

Figure 14: Total number of non escaping initial conditions (vertical axis) against integration time (horizontal axis) around the family VF3. Left: L_4 case. Right: L_5 case.

time. To try to show this dependence we have done the following calculation. To fix the discussion, let us focus on the L_4 point, and let O_j be the orbit on the family VF3 for which $\dot{z} = j/100$ when $z = 0$ ($j = 0, 1, 2, \ldots, 90$). Let $s_{n,j}$ be the number of non escaping initial conditions after n years (we are using the same mesh as before), around the orbit O_j. Let s_n be $\sum_j s_{n,j}$, that is, s_n denotes the total number of non escaping points around VF3. The values of s_n, for n ranging between 100 and 1000 years are displayed in Figure 14. We have tried several fittings on this data, trying to show the persistence of a certain number of points when n goes to infinity (see also [25]), but the results are inconclusive. It turns out that the amount of remaining points strongly depends on the fitting function used, and there are no theoretical reasons that suggest to pick up an especial kind of fitting function. We think that longer numerical integrations will help to elucidate this question.

3.2 Typical trajectories in the stable region

To explain the dynamics inside the quasi-stable region, we first show a few trajectories corresponding to the slices $\dot{z} = 0.58$ and $\dot{z} = 0.83$ (see Figure 11). In each slice, we have selected an initial condition near the “central part” of the slice. For each initial condition, we have computed the corresponding orbit in the JPL model, both for the L_4 and L_5 cases, and the results are displayed in Figures 15, 16, 17 and 18. To give a sense of velocity we have drawn the orbit as a polygonal line, putting a vertex for each day of integration.

It is interesting to look at the $(z, \dot{z})$ projection of these trajectories. They show that the vertical oscillations are very close to an harmonic oscillator: there is a clear frequency that dominates this motion and the remaining frequencies appear as a perturbation. This dominating frequency is already contained in the BCP and RTBP (it is related to the vertical frequency of the $L_{4,5}$ points in the RTBP and to the vertical frequency of the orbits PO1, PO2 and PO3 of the BCP), and its period is a little less than a month.

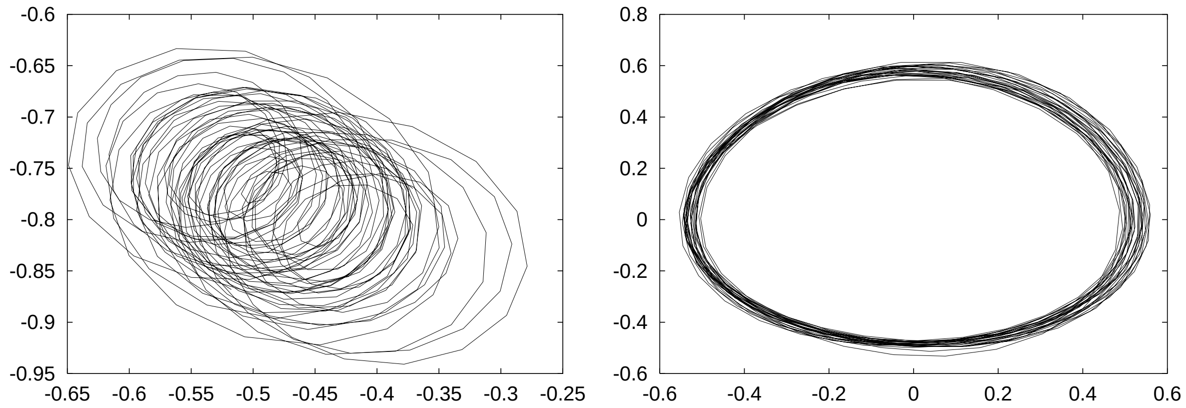

Figure 15: Trajectory inside the stability region of the JPL model, corresponding to the slice $\dot{z} = 0.58$ (L_4 case). Left plot: (x, y) projection; right plot: $(z, \dot{z})$ projection. Integration time: 2 years.

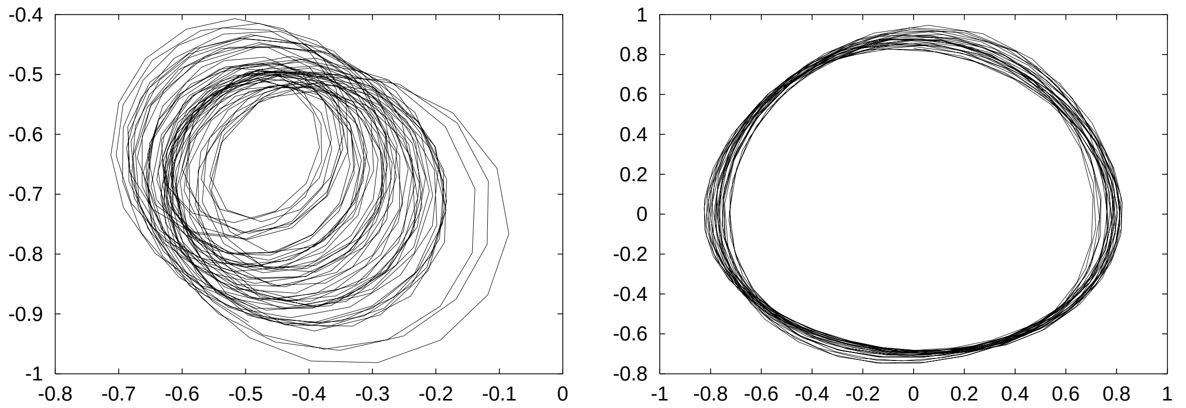

Figure 16: Trajectory inside the stability region of the JPL model, corresponding to the slice $\dot{z} = 0.83$ (L_4 case). Left plot: (x, y) projection; right plot: $(z, \dot{z})$ projection. Integration time: 2 years.

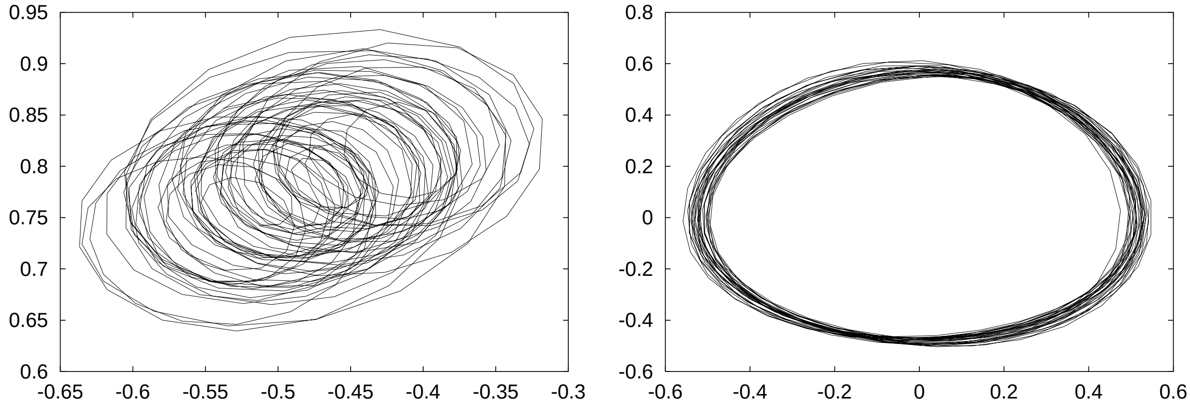

Figure 17: Trajectory inside the stability region of the JPL model, corresponding to the slice $\dot{z} = 0.58$ (L_5 case). Left plot: (x, y) projection; right plot: $(z, \dot{z})$ projection. Integration time: 2 years.

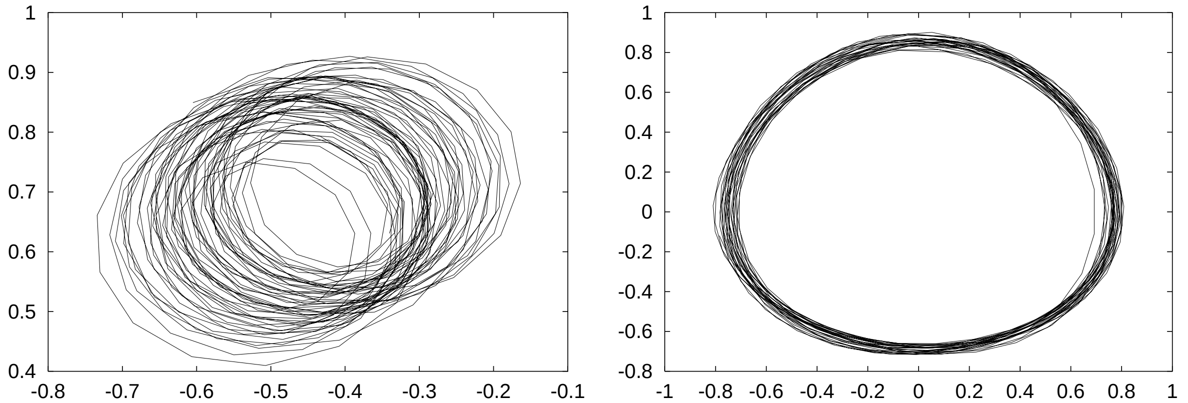

Figure 18: Trajectory inside the stability region of the JPL model, corresponding to the slice $\dot{z} = 0.83$ (L_5 case). Left plot: (x, y) projection; right plot: $(z, \dot{z})$ projection. Integration time: 2 years.

4 Technical details

This section contains some extra details on the metods used.

4.1 Numerical integrations

The numerical integrations for the BCP model have been done by means of a Taylor method of order 20 (see [20]), using the standard double precision of the computer. The local truncation error for the automatic step size control has been selected to be 10^{-16}. The numerical integrations for the JPL model have been done by a standard Runge-Kutta-Fehlberg of orders 7 and 8, with automatic step size control. The truncation error used has been 10^{-14}. Finally, a sample of the results shown in this work have been tested against a third numerical integrator, the Shampine-Gordon method, based on Adams formulas (for more details, see [23]). The results obtained are quite similar, with very small differences that seem to come from the different truncation errors of the methods.

4.2 Coordinate systems

Here we have mainly used two systems of reference. The first one is the standard coordinates of the RTBP and BCP (also called synodical coordinates), and the second one are the coordinates of the JPL ephemeris. From the data in the JPL ephemeris file we compute the equatorial coordinates of each planet (with origin at the instantaneous centre of masses of the Solar system), except for the Moon whose coordinates are referred to Earth. The numerical integrations for the JPL model are performed using the JPL coordinates. Note that, from a numerical point of view, it is not a good idea to have the origin of coordinates in the centre of masses of the Solar system because then the different coordinates of the trajectories near the triangular points of the Earth–Moon system are very similar, and this could result in cancellations of meaningful digits during the arithmetic operations. For this reason, the origin of coordinates has been translated to the Earth–Moon barycentre. The ideas for these tasks are described in [12], [13], [10] and [11].

5 Conclusions

One of the main issues of this work is to show the existence of regions of practical stability near the equilateral points of the real Earth–Moon system. It has been shown that the classical RTBP model is not enough for this study and, for this reason, we have used a suitable intermediate model, the BCP. The study of this model has revealed the existence of quasi-stable regions, but outside the Earth–Moon plane. Finally, these regions have been numerically checked against a realistic model of the Solar system obtained from the JPL ephemeris. In this way, we avoid doing massive numerical simulations on the JPL model that could result in a prohibitive need of computer time. The results show that a relevant part of the stable regions of the BCP persists in the JPL, at least for 1000 years.

A natural question is the persistence of these regions for longer time intervals. From the results presented here there is no a conclusive answer to this question. We are actually working in this direction by using improved versions of the BCP, taking into account Moon's eccentricity and inclination. The obtained regions for these models will be tested against longer numerical integrations of the Solar system. We believe that better models can give a deeper insight in many features of the dynamics, like the role played by resonances in the size and shape of these regions. Moreover, a more accurate determination of these regions should help to extend the quasi-stability times.

At this point we want to note that the JPL model is one of the most accurate models for the motion of the main bodies of the Solar system. In fact, the main sources of error when using the JPL to integrate the motion of a particle come from ignoring the non-Newtonian effects on this particle (like Solar wind or Solar radiation pressure), and from assuming that the mass of the bodies is concentrated in a single point. The latter issue is specially relevant when the particle comes close to these bodies but, in our case, this distance is quite big so that this effect can be considered as a very small (Hamiltonian) perturbation. It is well known (see [22] or [2]) that sufficiently small Hamiltonian perturbations have a small effect on the existence of quasi-stable regions.

One of the possible interests of the regions around the family VF3 is that they could be a suitable place to look for some kind of dust or even some small asteroids. In this case, it would not be very difficult to send a probe there to pick up some samples. Moreover, these regions plus the regions around the family VF2 could also be of interest for some space missions, since no control is necessary to keep a spacecraft there.

The typical motion for a particle inside this region has been shown in Figures 15–18. As it has been mentioned in Section 3.2, it is clear that the largest part of the region corresponds to trajectories that cut the Earth–Moon plane with vertical speeds (relative to that plane) close to either 0.58 or 0.83, in adimensional units. This corresponds to speeds close to either 0.56 or 0.80 Km/sec. We note that the motion in the vertical direction is very close to an harmonic oscillator (with a period of a little less than a month), and that these trajectories reach an approximate angular separation over (or under) the Earth–Moon plane of either 30 or 40 degrees. Hence, as it happens in a typical harmonic oscillator, the trajectories must spend most of the time away from the Earth–Moon plane and near their maximum elongation. Hence, to have the best chances to find Trojan asteroids in the Earth–Moon system one should focus the search around either 30 or 40 degrees over (and under) the Earth–Moon plane. Performing the search near that plane has much less chances of success and, even in this case, it can be difficult to confirm an observation since the asteroid is moving at its highest speed. In fact, there are records of a few observations of small dust clouds near the Earth–Moon Lagrangian points, but none of them has been confirmed later ([8]).

Acknowledgements

I am indebted with J. Masdemont for his version of the code developed in [12], [13], [10] and [11] to work with the JPL ephemeris. I also want to acknowledge interesting discussions with C. Simó. This research has been supported by the Spanish grant DGICYT PB94–0215 and the Catalan grant CIRIT 1998S0GR–00042. The numerical simulations

have been done on Hidra, the Beowulf cluster of the UB–UPC Dynamical Systems Group (see `http://www.maia.ub.es/dsg/hidra/`).

References

[1] V.I. Arnold. Instability of dynamical systems with several degrees of freedom. *Soviet Math. Dokl.*, 5:581–585, 1964.

[2] V.I. Arnold, V.V. Kozlov, and A.I. Neishtadt. *Dynamical Systems III*, volume 3 of *Encyclopaedia Math. Sci.* Springer, Berlin, 1988.

[3] G. Benettin, F. Fassò, and M. Guzzo. Nekhoroshev-stability of L_4 and L_5 in the spatial Restricted Three-Body Problem. *Regul. Chaotic Dyn.*, 3(3):56–72, 1998.

[4] E. Castellà and À. Jorba. On the vertical families of two-dimensional tori near the triangular points of the Bicircular problem. To appear in *Celestial Mech.*, 2000.

[5] A. Celletti and A. Giorgilli. On the stability of the Lagrangian points in the spatial Restricted Three Body Problem. *Celestial Mech.*, 50:31–58, 1991.

[6] V. Companys, G. Gómez, À. Jorba, J. Masdemont, J. Rodríguez, and C. Simó. Use of Earth-Moon libration points for future missions. In K.T. Alfriend, I.M. Ross, A.K. Misra, and C.F. Peters, editors, *AAS/AIAA Astrodynamics Conference*, volume 90 of *Advances in the Astronautical Sciences*, pages 1655–1666, San Diego, U.S.A., 1996. American Astronautical Society.

[7] C. Díez, À. Jorba, and C. Simó. A dynamical equivalent to the equilateral libration points of the real Earth-Moon system. *Celestial Mech.*, 50:13–29, 1991.

[8] R.A. Freitas and F. Valdes. A search for natural or artificial objects located at the Earth-Moon libration points. *Icarus*, 42:442–447, 1980.

[9] A. Giorgilli, A. Delshams, E. Fontich, L. Galgani, and C. Simó. Effective stability for a Hamiltonian system near an elliptic equilibrium point, with an application to the restricted three body problem. *J. Differential Equations*, 77:167–198, 1989.

[10] G. Gómez, À. Jorba, J. Masdemont, and C. Simó. Study refinement of semi-analytical Halo orbit theory. ESOC contract 8625/89/D/MD(SC), final report, European Space Agency, 1991.

[11] G. Gómez, À. Jorba, J. Masdemont, and C. Simó. Study of Poincaré maps for orbits near Lagrangian points. ESOC contract 9711/91/D/IM(SC), final report, European Space Agency, 1993.

[12] G. Gómez, J. Llibre, R. Martínez, and C. Simó. Station keeping of libration point orbits. ESOC contract 5648/83/D/JS(SC), final report, European Space Agency, 1985.

[13] G. Gómez, J. Llibre, R. Martínez, and C. Simó. Study on orbits near the triangular libration points in the perturbed Restricted Three–Body Problem. ESOC contract 6139/84/D/JS(SC), final report, European Space Agency, 1987.

[14] À. Jorba. On practical stability regions for the motion of a small particle close to the equilateral points of the real Earth–Moon system. Proceedings of the *III International Symposium HAMSYS-98. Geometrical Methods in Hamiltonian Systems and Celestial Mechanics.* Pátzcuaro (México), December 7–11, 1998. To appear.

[15] À. Jorba. Numerical computation of the normal behaviour of invariant curves of higher dimensional maps. In preparation, 2000.

[16] À. Jorba and C. Simó. Effective stability for periodically perturbed Hamiltonian systems. In J. Seimenis, editor, *Hamiltonian Mechanics: Integrability and Chaotic Behaviour*, volume 331 of *NATO Adv. Sci. Inst. Ser. B Phys.*, pages 245–252. Held in Toruń, Polland, 28 June–2 July 1993. Plenum, New York, 1994.

[17] À. Jorba and J. Villanueva. On the normal behaviour of partially elliptic lower dimensional tori of Hamiltonian systems. *Nonlinearity*, 10:783–822, 1997.

[18] À. Jorba and J. Villanueva. On the persistence of lower dimensional invariant tori under quasi-periodic perturbations. *J. Nonlinear Sci.*, 7:427–473, 1997.

[19] À. Jorba and J. Villanueva. Numerical computation of normal forms around some periodic orbits of the Restricted Three Body Problem. *Phys. D*, 114:197–229, 1998.

[20] À. Jorba and M. Zou. On the numerical integration of ODE by means of high-order Taylor methods. In preparation, 2000.

[21] K. R. Meyer and G. R. Hall. *Introduction to Hamiltonian Dynamical Systems and the N-Body Problem.* Springer, New York, 1992.

[22] N.N. Nekhoroshev. An exponential estimate of the time of stability of nearly-integrable Hamiltonian systems. *Russian Math. Surveys*, 32:1–65, 1977.

[23] L. F. Shampine and M. K. Gordon. *Computer solution of Ordinary Differential Equations.* Freeman, San Francisco, 1975.

[24] C. Simó. Estabilitat de sistemes Hamiltonians. *Mem. Real Acad. Cienc. Artes Barcelona*, 48(7):303–348, 1989.

[25] C. Simó, À. Jorba, J. Masdemont, and G. Gómez. The Bicircular model near the triangular libration points of the RTBP. In A.E. Roy and B.A. Steves, editors, *From Newton to Chaos*, pages 343–370, New York, 1995. Plenum Press.

[26] V. Szebehely. *Theory of Orbits.* Academic Press, 1967.

[27] `http://ssd.jpl.nasa.gov/horizons.html`.